(Received 21 February 2025, Accepted 1 April 2025, Scheduled 19 May 2025)

On-Body FSS-Backed High Gain Microwave System for Brain Tumor Diagnosis

Sanjeev Sharma[1], Daljeet Singh[2, 3], Mariella Särestöniemi[2, 3, 4], Teemu Myllylä[2, 3, 5, 6], and Rajeev Kumar[7, *]

[1]*Research Department, Rayat Bahra University, Mohali, Punjab 140104, India*
[2]*Research Unit of Health Sciences and Technology, Faculty of Medicine, University of Oulu, Oulu 90570, Finland*
[3]*Infotech Oulu, 90570, Finland*
[4]*Centre for Wireless Communications, Faculty of Information Technology and Electrical Engineering University of Oulu, Oulu 90570, Finland*
[5]*Opto-electronics and Measurement Technique Research Unit, Faculty of Information Technology and Electrical Engineering University of Oulu, Oulu 90570, Finland*
[6]*Medical Research Center (MRC) Oulu, University of Oulu, Oulu 90570, Finland*
[7]*Chitkara University Institute of Engineering and Technology, Chitkara University, Punjab, India*

ABSTRACT: The paper presents a microwave system operating at 4–5 GHz for brain tumor diagnosis. The proposed work presents a novel method to detect the presence of tumors by capitalizing on the variations in antenna response. To achieve highly precise and fast diagnosis, a high-gain antenna is placed on the surface of the skull. The gain and directivity of the antenna are enhanced by using a Frequency selective surface (FSS) array structure placed behind the antenna which directs the energy towards the human tissues for tumor detection purposes. By using the FSS array surface, there is a 4.3 dB increase in gain and a 4.2 dB increase in directivity. Simulations are carried out using a multi-layer skull model comprising Skin, Skull, and Brain. Our proposed work demonstrates that there is a variation of about 8 dB in S-parameters when a tumor of size 6 mm $\times$ 6 mm is placed in the brain area. Further, we have investigated the S-parameter characteristics using different shapes and sizes of tumors in the brain. The results show that variation in S-parameter characteristics can be potentially used to detect the presence of tumors in the human brain.

1. INTRODUCTION

In recent years, brain tumors and other brain-related diseases have become a colossal burden on healthcare and are one of the leading causes of disability and death. A brain tumor is a very serious condition wherein the key tissues of the brain are affected, often causing irreversible damage to the overall cognition and health of the brain. If not diagnosed and treated in time, brain tumors can transform into brain cancer as a result of abnormal cell development inside the brain. Shockingly, brain tumors are the 9^{th} main cause of death among humans [1]. The benign tumor is non-cancerous and does not harm other parts of the body; however, once transformed into a malignant tumor, it rapidly spreads across the body affecting its vital functionality. Luckily, if diagnosed timely, brain tumors can be treated like other tumors, thereby improving the chances of patient survival. Medical research has evolved with time, and a lot of modalities are proposed for brain tumor diagnosis including ultrasound, computed tomography (CT), X-ray imaging, magnetic resonance imaging (MRI), biopsy, positron emission tomography (PET) scans, etc. However, all of these techniques are expensive, labor intensive, and often involve gigantic hardware limiting its use to only specialized hospitals. On the other hand, Microwave techniques are proven to be more useful for time-critical situations at remote locations where access to these traditional modalities is not available [2]. Microwave systems are low power consuming, have planar low-profile structures, are cost-effective, can penetrate deeper into the body, and are non-ionizing in nature, therefore making them a very suitable candidate for brain tumor diagnosis [3, 4]. Microwaves are also utilized extensively for brain tumor treatment (Microwave Hyperthermia) [5–8] and for tumor diagnosis in other areas of the body such as breast [9, 10], lungs [11], and other areas [12, 13].

Rodriguez et al. [14] presented a brick-shaped antenna for brain imaging applications. The antenna operated at 800 MHz–1.2 GHz and was tested on head phantom models. Further, authors in [15] developed a metamaterial-based antenna array for brain imaging applications. The multilayer antenna array was fabricated using Rogers RT5880 and RO4350B substrates with nine elements in an array. In a similar work, Hamza et al. [16] proposed a microwave system embedded with an artificial magnetic conductor for brain tumor diagnosis with a resonant frequency of 2.276 GHz. Apart from these metamaterials-based solutions, a deep transfer learning model is presented in [17] for brain tumor classification which achieves an accuracy of 99.65% and f score of 99.23%. The model consists of five layers and is tested on a dataset with 4200 images.

Authors in [18] presented a slotted microstrip patch antenna for brain tumor diagnosis using S parameter analysis. The pro-

* Corresponding author: Rajeev Kumar (rajeev_chauhan364@yahoo.co.in, rajeev.kumar@chitkara.edu.in).

posed antenna in [18] operated at 6–10 GHz. The system was also tested for its specific absorption rate (SAR) which was found to be 2.53×10^6 w/m^3. Chandra and Balasingham [19] devised a finite-difference-time-domain (FDTD) simulation-based microwave system for brain tumor detection operating at 403.5 MHz band. The authors show that a threshold of 45 dB signal-to-noise ratio (SNR) is essential for the diagnosis of small-size tumors. A microwave system with a bandwidth of 1.59 to 5.2 GHz is presented in [20] which is tested on a seven-layer model using simulations in CST microwave studio. Särestöniemi et al. [4] proposed digital twins (DTs) for brain tumor detection using microwave systems. Anatomically accurate models based on MRI scans are developed and tested in this study for their efficiency in brain tumor diagnosis. The system was tested using flexible ultra-wideband (UWB) antennas of size 40×40 mm operating at 2–10 GHz. These DTs can be optimized as per user specifications to suit specific cases of brain tumor size, location, and severity. A metamaterial (MTM) loaded 3D stacked antenna array is proposed by Hossain et al. [15]. The design consists of a 1×4 MTM array element on top and a 3×2 MTM array element in the bottom layer which is fabricated by Rogers RT5880 and RO4350B substrates. The operational bandwidth of this system is 1.37–3.16 GHz.

Several emulation models for microwave system evaluation are presented in [21]. These 3D emulation models are proposed for different conditions such as tumors, strokes, and cancers. A near-field microwave radiometry system for passive brain tumor detection is proposed by Groumpas et al. in [22]. The passive system of [22] operated at 1.5 GHz with a four-port total power Dicke-switch at its heart. Authors in [23] presented a method for brain tumor classification using reconstructed microwave brain (RMB) images. Six different classes of tumors were used as reference cases in this study. In [20], a star-shaped patch antenna is designed for brain tumor diagnosis. The operational bandwidth of the system is 1.47–4.7 GHz with a peak gain of 3.8 dBi. Delay and Sum algorithm is utilized in this work for tumor localization. Inum et al. [24] proposed an electromagnetic band gap (EBG) structure for detecting brain tumors. The proposed design is 22.77% more efficient in terms of return loss and 5.84% more in impedance bandwidth with respect to its non-EBG counterpart.

The present study presents a noninvasive microwave system for brain tumor diagnosis from the skin of the subject. The proposed system operates at a frequency band of 4–5 GHz. A novel method is utilized to detect the presence of tumors by capitalizing on the variations in antenna response. A high-gain antenna is placed on the surface of the skull for tumor diagnosis, and a very precise as well as real-time diagnosis is achieved. The gain and directivity of the antenna are enhanced by using a unique frequency selective surface (FSS) array structure placed behind the antenna which directs the energy towards the human tissues to improve the antenna gain by 4.31 dB and directivity by 4.2 dB. Simulations are carried out using a multi-layer skull model comprising Skin, Skull, and Brain. The results obtained by simulations and measurements on realistic human head phantoms demonstrate that even a very small tumor of any shape can be diagnosed with high accuracy using the proposed system. The rest of the paper is organized as follows. Section 2 presents the material and methods utilized in this work including the microwave system design, parametric analysis for optimization, and on-body trials. Section 3 presents the results and discussion of both simulation and measurement trials. The characteristics of the proposed antenna with different tumor shapes and sizes are analyzed in this section. Section 5 holds the concluding remarks of the paper.

2. MATERIAL AND METHODS

This section presents the materials and methods utilized in this work. The antenna is designed using a Roger RT/Duroid 5880 substrate, and FSS is fabricated on an FR4 substrate. The parametric analysis to evaluate antenna placement over FSS is also presented in this section along with the combined FSS array-antenna setup and fabrication process. The designed antenna is tested on realistic human-head phantoms. The process of phantom preparation and testing is described in the following subsections with details of on-body trials and simulation setup.

2.1. Microwave Antenna Design

The proposed microwave system consists of a planar microwave antenna of overall dimensions 36 mm $\times$ 35 mm. The width of the planar microwave antenna is extended to 56 mm to support the FSS structure. The antenna uses a Roger RT/Duroid 5880 substrate with 0.51 mm thickness and dimensions of 56 mm $\times$ 35 mm. The feedline has a semi-circle of 8.5 mm radius placed on top of a feedline of dimensions 11 mm $\times$ 2 mm. There are two rectangular structures of 6.75 mm $\times$ 13 mm and 4 mm $\times$ 7 mm on top of the semi-circle, as shown in Fig. 1. The antenna has been extended by 10 mm on either side to accommodate four screws for holding the support rods between the FSS array and antenna. The ground plane has an elliptical cut on its upper part and a thin strip surrounding the antenna in dark blue color as shown in Fig. 1.

2.2. FSS Unit Cell Design

The second main component of the microwave system is a Frequency Selective Surface which further optimizes the proposed system. The FSS unit cell is designed on an FR4 substrate with dimensions of 15 mm $\times$ 15 mm $\times$ 1.6 mm. The unit cell consists of an outer square of 14.6 mm $\times$ 14.6 mm. An inner circle of radius 4.75 mm is etched out from the outer square as shown in Fig. 2(a). The simulation is done by creating a two-port Floquet setup in HFSS software which is depicted in Fig. 2(b). To meet the specific requirements of the application, the design of the FSS array should cover the frequency bandwidth of interest, and the return loss should be adequate in this range. The optimum frequency band of operation for detecting tumors is selected as 4–5 GHz. So, both the antenna and FSS array should operate in this frequency range. The unit cell optimization is carried out through an iterative process, systematically varying the circle's radius (R) as well as the length and breadth of the unit cell. After multiple iterations, the optimal design is achieved with a circle radius of $R = 4.75$ mm and a square unit cell measuring 11 mm $\times$ 11 mm. It can be visualized from

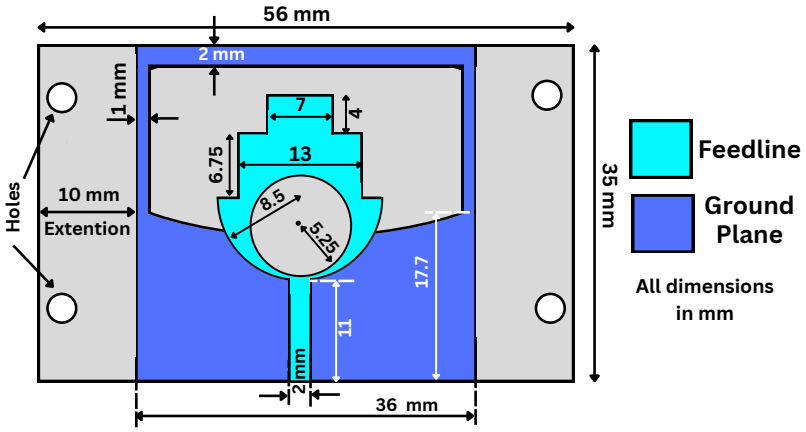

FIGURE 1. Schematic diagram of proposed antenna design showcasing feedline and ground plane.

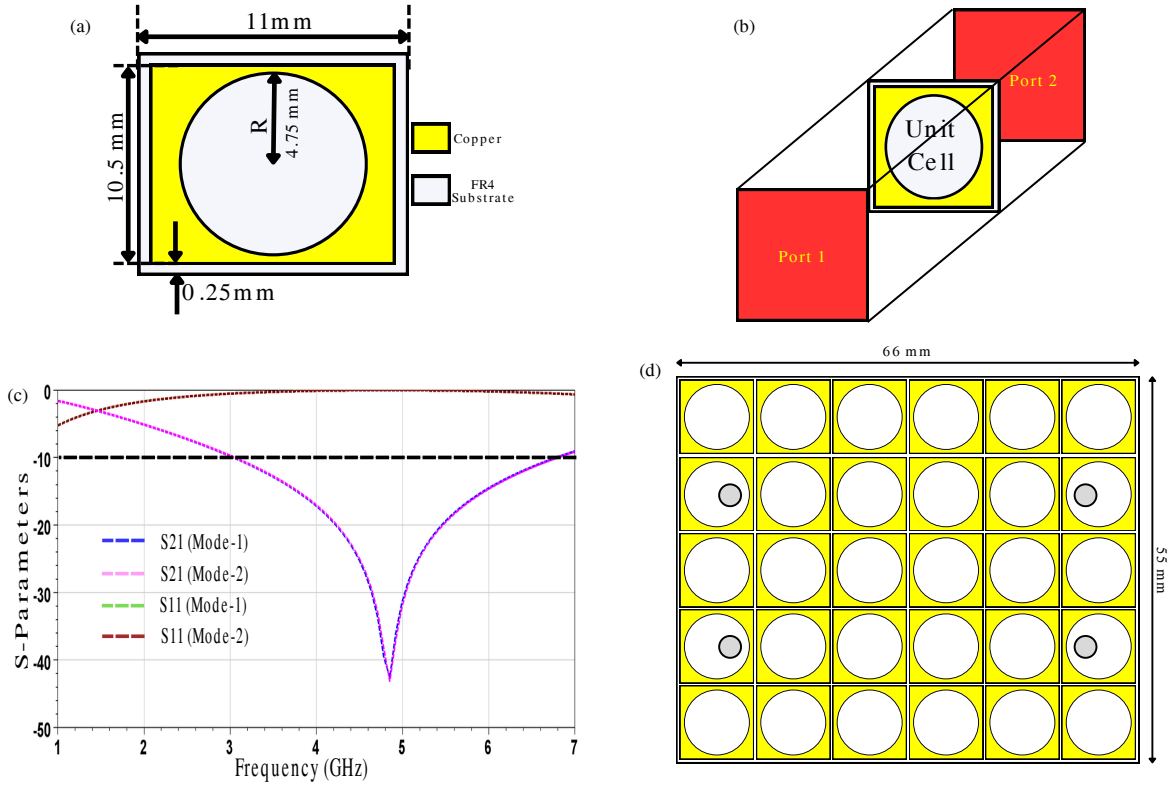

FIGURE 2. FSS design. (a) Unit cell. (b) Port configuration. (c) S parameter analysis of unit cell, and (d) FSS array.

Fig. 2(c) that the S_{21} characteristics of the unit cell are designed to cover a wide frequency band from 3.1 GHz to 6.7 GHz with a center frequency of 4.9 GHz. It means that the incident electromagnetic waves on the FSS surface will be reflected in this frequency range and will overlap and combine with the incident wave to create a stronger signal. Consequently, the use of FSS helps in focusing the electromagnetic energy of the antenna in the desired direction which results in improving several antenna parameters, such as gain, directivity, and front-to-back-ratio (FTBR).

The designed FSS unit cells are repeated to form an FSS array. An array of 5 × 6 unit cells is formed with an overall dimension of 66 mm × 55 mm as shown in Fig. 2(d). Each unit cell is separated from the adjacent unit cell by a 0.5 mm distance. Additionally, four holes are drilled for holding support rods between the FSS plate and antenna. These holes are precisely aligned with the corresponding holes in the antenna so that the exact positioning of FSS and antenna is ensured.

The overall FSS structure with holes marked in grey is shown in Fig. 2(d).

2.3. Parametric Analysis of Antenna Placement over FSS

The separation between the antenna and FSS structure is a critical design parameter that significantly influences key antenna

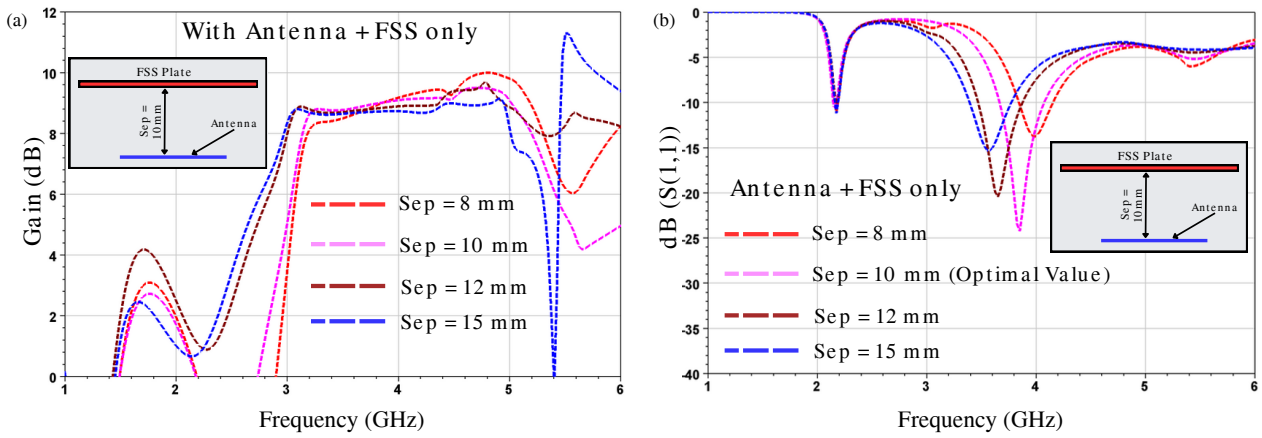

FIGURE 3. Effect of separation between antenna and FSS (Sep) on: (a) Gain, (b) S-parameters.

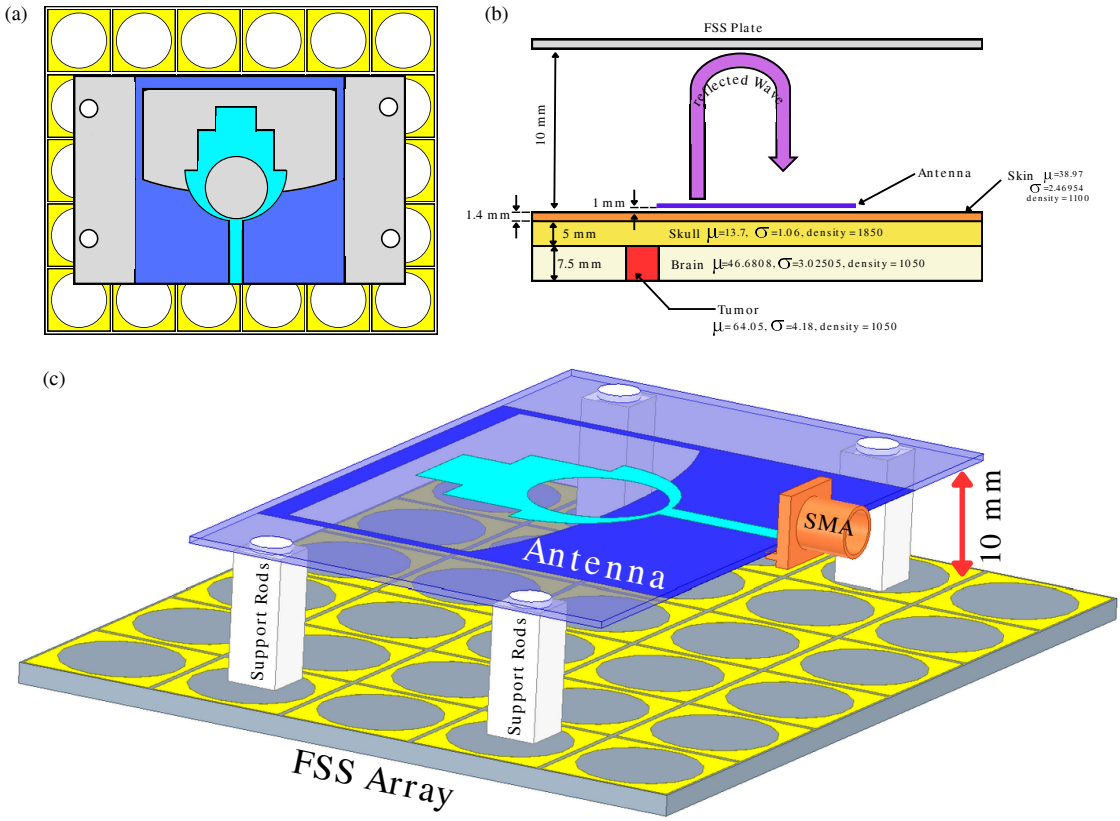

FIGURE 4. Combined structure. (a) Top view. (b) Side view. (c) 3-D view.

performance metrics, such as matching characteristics, radiation pattern, and gain. To ensure optimal system performance, a thorough parametric analysis is conducted in this section to study the impact of varying the height between the antenna and FSS structure. This analysis reveals the specific trends and trade-offs associated with the antenna's performance as a function of the separation distance. An iterative optimization process determines the distance of separation (Sep) between the antenna and FSS plate. The distance "Sep" has been varied from 8 mm to 15 mm to get an optimal value for gain and S-parameters. The variation analysis is shown in Fig. 3. It can be observed from Fig. 3(a) that in the frequency band of interest, by changing the distance of separation (Sep) there is not much variation in the gain. However, it has a strong impact on the S-parameters as shown in Fig. 3(b). Therefore, a value of Sep = 10 mm is chosen as it provides optimal return loss and gain.

2.4. Combined FSS Array and Antenna Setup

The top view of the alignment of FSS plate and antenna is shown in Fig. 4(a). The FSS array surface is placed 10 mm above the antenna ground plane surface as shown in Fig. 4(b). The combined FSS and antenna structure is placed at a dis-

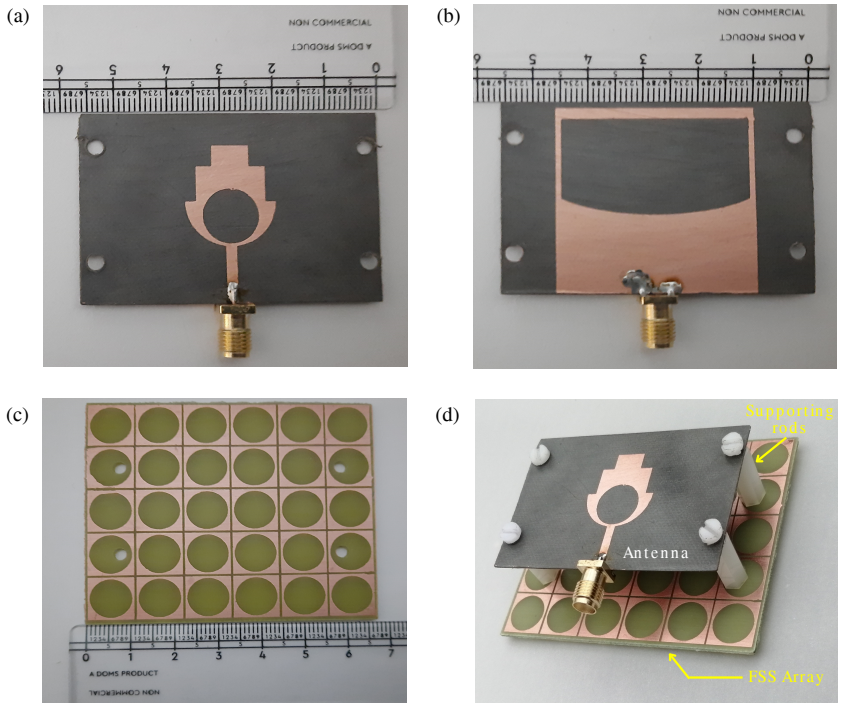

FIGURE 5. Fabricated prototype: (a) Antenna feed plane. (b) Antenna ground plane. (c) FSS array. (d) Combined FSS-antenna.

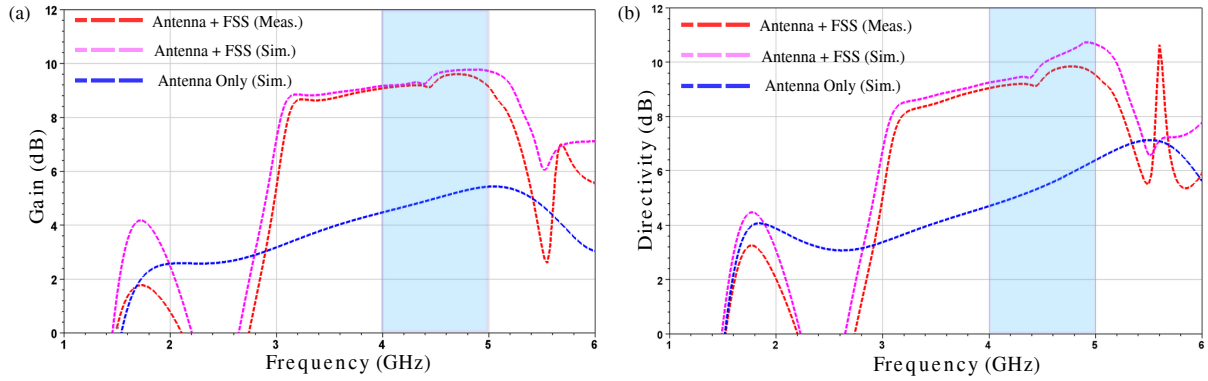

FIGURE 6. Combined antenna and FSS characteristics. (a) Gain. (b) Directivity.

tance of 1 mm from the layered phantom model comprising three layers: skin, skull, and brain. The placement of the antenna and FSS with respect to layered phantom model is shown in Fig. 4(b) along with their thickness and corresponding dielectric properties. The thickness of the skin, skull, and brain is taken as 1.4 mm, 5mm, and 7.5 mm respectively. The position of the tumor marked in red color is also shown in Fig. 4(b). The three-dimensional arrangement of the antenna and FSS array is visualized in Fig. 4(c). The combination of the proposed antenna and FSS results in enhanced system performance.

The fabricated prototype of the FSS-antenna combination is shown in Fig. 5. The antenna feed plane is visualized in Fig. 5(a) whereas the ground plane is shown in Fig. 5(b). The FSS array fabricated for the designed antenna is shown in Fig. 5(c). The antenna and FSS array plate are firmly supported by Teflon support rods and fixed with Teflon screws as shown in Fig. 5(d) which shows the combined arrangement of the FSS-Antenna. This arrangement not only provides rigidity to the overall structure but also helps to precisely align the antenna and FSS array plate to get the desired results.

The gain of the combined structure increases by 4.3 dB compared with only the antenna structure as shown in Fig. 6(a). Further, the directivity of the combined structure is also enhanced by 4.2 dB which is shown in Fig. 6(b). The increase in gain and directivity helps to direct the electromagnetic energy of microwave structure in the desired direction. A comparative far-field radiation pattern with only the antenna and a combined Antenna-FSS structure is shown in Fig. 7. The comparative results with and without FSS depict the influence of deploying the FSS array behind the antenna. The radiation pattern shows the narrower and directional nature of the main lobe and scaling down of the back lobe. The reshaping of radiation pattern due to the deployment of FSS behind antenna leads to the enhancement of gain and directivity. The directional and

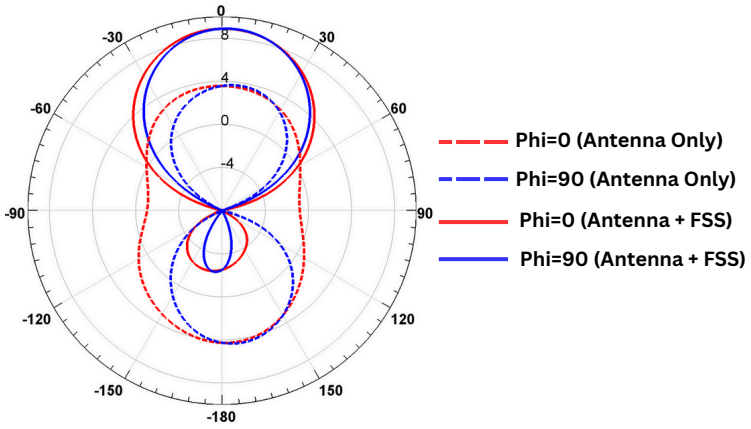

FIGURE 7. Radiation pattern of only antenna and antenna + FSS structure at 3.9 GHz.

narrower main lobe supports deeper penetration into the brain for tumor detection.

2.5. On-Body Trials

This subsection presents a detailed description of the simulation and measurement setup undertaken in this work for testing the proposed antenna for brain tumor monitoring. The gain and directivity of the designed antenna are enhanced by using an FSS array. A setup consisting of an antenna and FSS array is utilized to measure the S-parameters on the human head phantom model comprising skin, skull, and brain layers. A detailed description of the phantom preparation process is available in [4]. Although the detailed procedure is mentioned in [4], the broad outline of the steps involved in phantom preparation is as mentioned below:

1. Step-1: For brain phantom preparation, water is initially heated up to 65°C. Geltin is added to the water when 65°C temperature is reached to make water+gelatin solution. Oil which is separately preheated to 50°C is added to the water+gelatin solution along with dishwashing liquid. The solution is slowly stirred and heated again to 65°C.

2. Step-2: The mixture created in step-1 is poured in two molds which gets solidified after cooling to room temperature.

3. Step-3: In one of the mold, tumor phantom is inserted. The recipe for the preparation of tumor phantom is mentioned in [4].

4. Step-4: Once both molds solidify upon cooling, the solidified phantoms are removed from both mold shells, which can be further used for testing with antenna.

5. Step-5: Detection of the tumor is carried out by comparing the measured S parameters of the two molds.

The FSS-Antenna setup is placed on the surface of the human head phantom to capture simulation as well as measurement results. The five steps for phantom preparation and measurements utilized in testing proposed microwave antenna are shown in Fig. 8. Reading of S_{11} is taken in two scenarios, first without any tumor and then in the presence of a tumor in brain area of head. The variation in the S-parameters characteristics is exploited to detect the presence of tumor.

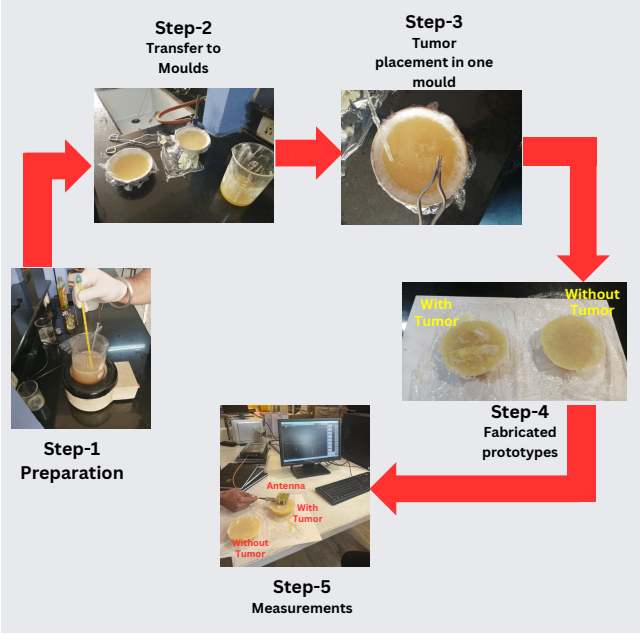

FIGURE 8. Steps for phantom preparation and measurements utilized in testing proposed microwave antenna.

The S_{11} characteristics under four different scenarios are depicted in Fig. 9(a). A detailed description of these scenarios is as follows:

Scenario-1 (With Antenna Only): Antenna resonates at 2.2 GHz with narrow bandwidth.

Scenario-2 (With Antenna and FSS combination): In this scenario, in-order to enhance the gain and directivity, an FSS array plate is placed at the back of the antenna. The S_{11} plot for Antenna and FSS combination shows resonance at two different frequencies. One at 2.15 GHz and the other at 3.8 GHz.

Scenario-3 (With Antenna, FSS, and Human Body): In Scenario 3, the Antenna-FSS combination is placed at 1 mm

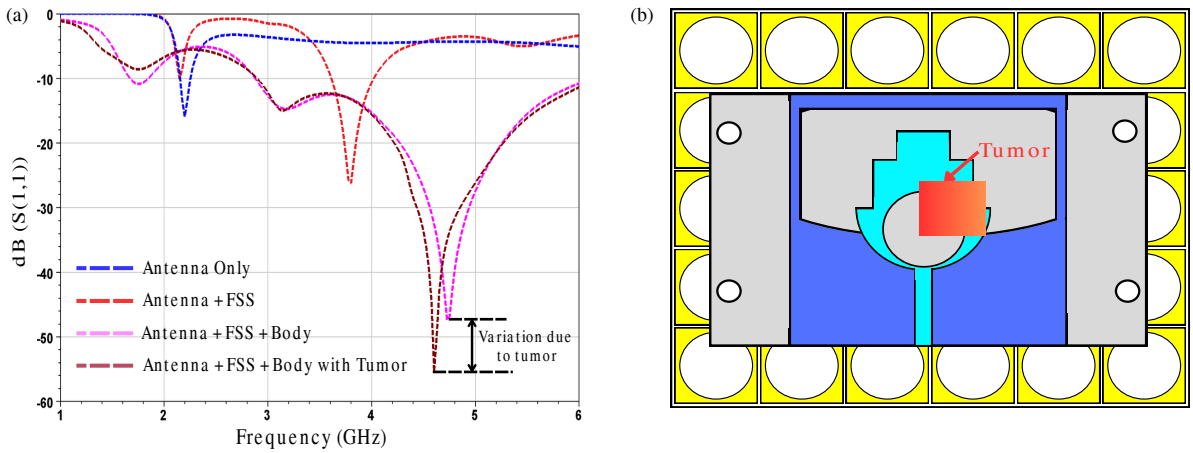

FIGURE 9. (a) S_{11} characteristics under four different scenarios. (b) Tumor alignment with antenna (Top View).

separation from the skin surface which is shown in Fig. 4(b). In this scenario, there is no tumor in the brain area of head. It can be seen that there is a shift in resonance frequency from 3.8 GHz to 4.75 GHz along with a sharp dip in S_{11} characteristics. Also, the S_{11} plot shows a substantial increase in bandwidth as shown in Fig. 9(a).

Scenario-4 (With Antenna, FSS, Human Body with Tumor): In this scenario, a tumor of size 6 mm × 6 mm × 7.5 mm is inserted in the brain area as shown in Fig. 9(b). It is observed that when the tumor is aligned at the position as depicted in Fig. 4(b) and Fig. 9(b), the combined structure resonates sharply at 4.6 GHz frequency with −56 dB return loss. It can be seen that the return loss which was earlier −46 dB without tumor has now fallen to −56 dB with the insertion of tumor. This variation of nearly 10 dB in S_{11} characteristics with the addition of a tumor can be potentially exploited to indicate the presence of tumors inside a human brain.

3. RESULTS AND DISCUSSIONS

The proposed microwave system is tested on realistic phantom models using simulations in HFSS with Finite Element Method (FEM) and bio-mimicking phantom models described in Subsection 2.5. The following subsections present the results obtained by simulation and measurements of different tumor shapes and sizes.

3.1. Effect of Tumor Shape

To study the effect of tumor shape, three different tumor geometries are undertaken: spherical, cubical, and cylindrical-shaped tumors. The proposed antenna is tested using spherical, cubical, and cylindrical tumor shapes as shown in Figs. 10(a), (c), (e). It can be visualized from Figs. 10(a), (c), (e) that all three tumor shapes show notable variation in S-parameters when the tumor is inserted in the brain layer. The relative position and size of the tumor are shown in the inset of Figs. 10(a), (c), (e). For a spherical tumor of a 3 mm radius, the return loss decreased to about −57 dB with the presence of a tumor as shown in Fig. 10(a). Without the tumor, the return loss was earlier −46 dB, with other conditions remaining the same. Similarly, as shown in Fig. 10(c), for a cube-shaped tumor of size 6 mm × 6 mm, the return loss which was earlier about −46 dB without the tumor is now decreased to −56 dB with the presence of a tumor. The presence of a cylinder-shaped tumor, as shown in Fig. 10(e), also depicts a sharp dip of −60 dB in return loss.

3.2. Effect of Tumor Dimensions

The simulated results for the sphere-shaped tumor are shown in Fig. 10(b). The radius (R) of the spherical tumor is varied, and simulated S-parameters are captured. It can be visualized from Fig. 10(b) that when the tumor radius is increased, there is a sharp decrease in return loss. With a spherical tumor of radius 2.5 mm, the captured return loss is about −54 dB which further decreases to −57 dB when the radius of the tumor is increased to 3 mm. With a further increase of tumor radius to 3.5 mm, the return loss decreases to −62 dB. Similarly, for cubical-shaped tumors which are placed as shown in Fig. 10(d) (inset), the S-parameters also show variation with respect to the size of a tumor. The tumor size is varied in size from 5 mm × 5 mm, 6 mm × 6 mm, and 7 mm × 7 mm. It can be seen from Fig. 10(d) that as the size of the tumor increases, there is a larger dip in simulated S-parameters. For a 5 mm × 5 mm-sized cubical tumor, the S_{11} dips to a value of −54 dB. As the size of the tumor is increased to 6 mm × 6 mm, the S_{11} dips further to −56 dB. With a 7 mm × 7 mm sized tumor, there is S_{11} dips substantially to a value of −69 dB. A tumor of cylindrical shape of radius 3.5 mm is placed as shown in Fig. 10(f) (inset). The length "L" of the cylindrical tumor is varied from 9 mm to 11 mm, and it is observed that the dip in S_{11} increases with the increase in length L of the cylinder. With a cylindrical tumor of length $L = 9$ mm, the return loss is about −50 dB which further decreases to −54 dB when the length of cylindrical tumor is increased to 10 mm. With $L = 11$ mm, the return loss further dips to about −60 dB as depicted in Fig. 10(f).

To further validate the practical applicability of the proposed system, we conducted phantom trials using bio-mimicking models of healthy human brains and brains with tumors of different sizes and shapes. The measurement results of phantoms with and without tumor using the proposed microwave antenna

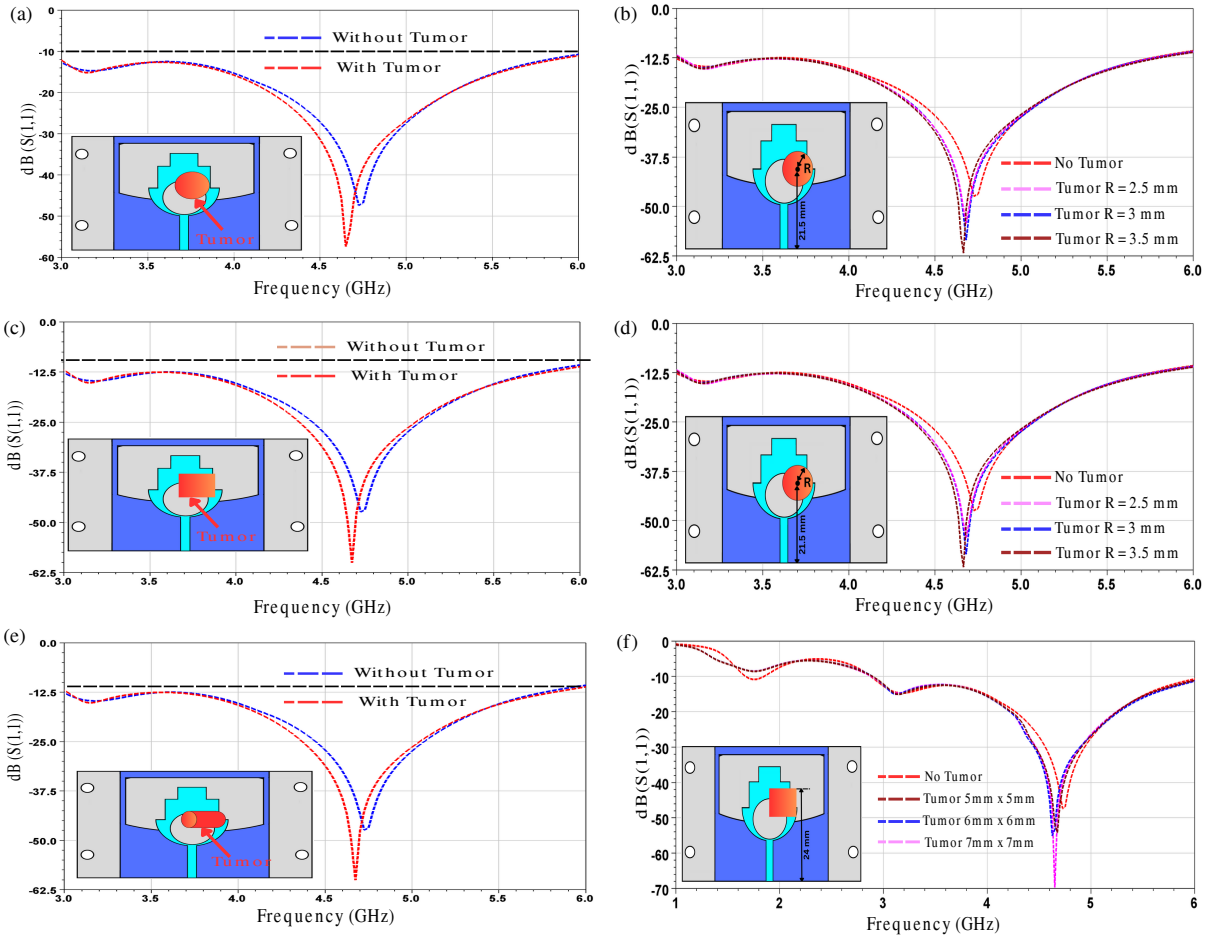

FIGURE 10. S-parameters with different tumor shapes. (a) Spherical. (c) Cubical. (e) Cylindrical; and variation of S-parameters with: (b) radius (R) of Sphere, (d) dimensions of cube, (f) length (L) of Cylinder tumors.

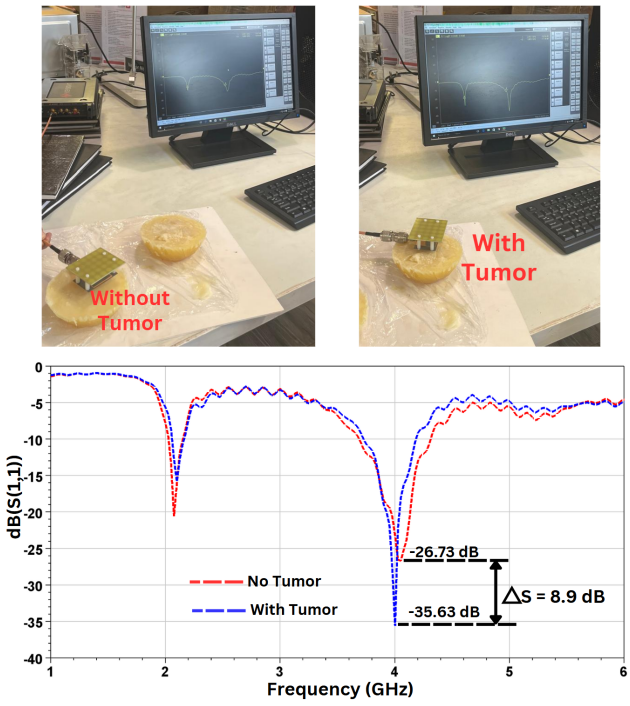

FIGURE 11. Measurement results on brain phantom with and without tumor using proposed microwave antenna.

TABLE 1. Comparative analysis of proposed antenna design with state-of-the-art literature.

Ref	Antenna Design	Dimensions (mm)	Frequency (GHz)	Method	Results
[25]	Rectangular UWB	27.6×29.15	6–8.5	Current density, S_{11}	Current density & S_{11} variation with/without tumor
[26]	Single element UWB	$44 \times 30 \times 1.4$ (FR4)	3.35–12.6	Deviation in Frequency	$\Delta f = 213$ MHz with/without tumor
[27]	Pentagon shaped patch	$33 \times 23 \times 1$ (FR4)	2.4–2.4835	S_{11} & E-field variation	Minor variation S_{11} & E-field with/without
[28]	4×1 array	$200 \times 78 \times 1.6$ (FR4)	2.4–2.45	S_{11} magnitude variation	21 dB increase in S_{11} over no-tumor scenario
[29]	Two Cross-slot antenna	$70 \times 47 \times 1.6$ (FR4)	1.8–3	S_{21} variation & echo state detection on minced chicken	77.5% testing accuracy
[30]	UWB MIMO	$30 \times 40 \times 1.6$ (FR4)	2.8–20	S_{11}, S_{22}, S_{33}, S_{44}, S_{41}, & S_{31} magnitude & Phase variation	Unsupervised machine learning
[31]	4×1 array (circular polarization)	$200 \times 78 \times 1.6$ (FR4)	2–3	S_{11} & frequency shift	$\Delta S_{11} = 5$–16.6 dB & $\Delta f = 2$–28 MHz
[32]	Monopole antenna	$17.5 \times 17.5 \times 0.8$ (RT/Duroid-5880)	2.4	S_{11} variation	$\Delta S_{11} = 12$ dB with/without kidney stone
Proposed	FSS-backed high gain antenna (36×35 mm)	Ant - $36 \times 35 \times 0.51$ (RT/Duroid 5880)	4–5	S_{11} variation, realistic phantom trials on tumor shapes: Spherical, Cubical, Cylindrical	$S_{11} = -56$ dB with tumor of size 6×6 mm

are shown in Fig. 11. These trials demonstrate that the antenna's response shows a distinctive change when being tested with and without a tumor. This consistent and measurable change underscores the suitability of the proposed microwave antenna for real-world applications in brain tumor diagnosis. A comparative analysis of the proposed antenna design with state-of-the-art literature is presented in Table 1.

4. CONCLUSIONS

In this paper, a novel method has been proposed to detect the presence of tumors in human brain by the use of variation in S-parameters of antenna. This is accomplished by the use of a high-gain antenna which is placed on the surface of skull. The requirement of high gain and directivity of the antenna is achieved by the use of an FSS array which is placed behind the antenna and directs the energy towards the human tissues for tumor detection purposes. Simulation results for S-parameters with different shapes and sizes have been investigated. The results show that the variation in S-parameter characteristics can be potentially used to detect the presence of tumors in the human brain. In the future, digital twin technology will be utilized to create a digital twin of the proposed microwave system for brain tumor diagnosis applications. The designed antennas will also be tested for other biomedical applications such as skull fracture detection, the study hydrodynamics of the brain, and in traumatic brain injury (TBI) cases. The antenna design can be further developed to multiple-input multiple-output (MIMO) configuration for imaging applications.

REFERENCES

[1] Tariq, M., A. A. Siddiqi, G. B. Narejo, and S. Andleeb, "A cross sectional study of tumors using bio-medical imaging modalities," *Current Medical Imaging*, Vol. 15, No. 1, 66–73, 2019.

[2] Singh, D., E. Vihriälä, M. Särestöniemi, and T. Myllylä, "Microwave technique based noninvasive monitoring of intracranial pressure using realistic phantom models," in *Nordic Conference on Digital Health and Wireless Solutions*, 413–425, 2024.

[3] Alqadami, A. S. M., K. S. Bialkowski, A. T. Mobashsher, and A. M. Abbosh, "Wearable electromagnetic head imaging system using flexible wideband antenna array based on polymer technology for brain stroke diagnosis," *IEEE Transactions on Biomedical Circuits and Systems*, Vol. 13, No. 1, 124–134, 2018.

[4] Särestöniemi, M., D. Singh, C. Heredia, J. Nikkinen, M. Von Und Zu Fraunberg, and T. Myllylä, "Digital twins for development of microwave-based brain tumor detection," in *Nordic Conference on Digital Health and Wireless Solutions*, 240–254, 2024.

[5] Winter, A., J. Laing, R. Paglione, and F. Sterzer, "Microwave hyperthermia for brain tumors," *Neurosurgery*, Vol. 17, No. 3, 387–399, 1985.

[6] Redr, J., T. Pokorny, T. Drizdal, O. Fiser, M. Brunat, J. Vrba, and D. Vrba, "Microwave hyperthermia of brain tumors: A 2D assessment parametric numerical study," *Sensors*, Vol. 22, No. 16, 6115, 2022.

[7] Dewhirst, M. W., B. L. Viglianti, M. Lora-Michiels, M. Hanson, and P. J. Hoopes, "Basic principles of thermal dosimetry and thermal thresholds for tissue damage from hyperthermia," *International Journal of Hyperthermia*, Vol. 19, No. 3, 267–294, 2003.

[8] Lyons, B. E., R. H. Britt, and J. W. Strohbehn, "Localized hyperthermia in the treatment of malignant brain tumors using an interstitial microwave antenna array," *IEEE Transactions on Biomedical Engineering*, Vol. BME-31, No. 1, 53–62, 1984.

[9] Särestöniemi, M., D. Singh, J. Reponen, and T. Myllylä, "Tailored 3D breast models for development of microwave based breast tumor screening," *Finnish Journal of eHealth and eWelfare*, Vol. 16, No. 1, 23–34, 2024.

[10] Benny, R., T. A. Anjit, and P. Mythili, "An overview of microwave imaging for breast tumor detection," *Progress In Electromagnetics Research B*, Vol. 87, 61–91, 2020.

[11] Muhammad, S. N., M. M. Isa, and F. Jamlos, "Review article of microwave imaging techniques and dielectric properties for lung tumor detection," in *AIP Conference Proceedings*, Vol. 2203, No. 1, 2020.

[12] Selvaraj, V., J. B. J. J. Sheela, R. Krishnan, L. Kandasamy, and S. Devarajulu, "Detection of depth of the tumor in microwave imaging using ground penetrating radar algorithm," *Progress In Electromagnetics Research M*, Vol. 96, 191–202, 2020.

[13] Gong, Z., Y. Chen, X. Lin, and M. J. Cree, "Contrast-enhanced microwave cancer detection using angle-of-arrival approach," *IEEE Transactions on Antennas and Propagation*, Vol. 70, No. 5, 3772–3780, 2021.

[14] Rodriguez-Duarte, D. O., J. A. T. Vasquez, R. Scapaticci, L. Crocco, and F. Vipiana, "Brick-shaped antenna module for microwave brain imaging systems," *IEEE Antennas and Wireless Propagation Letters*, Vol. 19, No. 12, 2057–2061, 2020.

[15] Hossain, A., M. T. Islam, G. K. Beng, S. B. A. Kashem, M. S. Soliman, N. Misran, and M. E. H. Chowdhury, "Microwave brain imaging system to detect brain tumor using metamaterial loaded stacked antenna array," *Scientific Reports*, Vol. 12, No. 1, 16478, 2022.

[16] Hamza, M. N., M. T. Islam, and S. Koziel, "Advanced sensor for non-invasive breast cancer and brain cancer diagnosis using antenna array with metamaterial-based AMC," *Engineering Science and Technology, An International Journal*, Vol. 56, 101779, 2024.

[17] Hossain, A., R. Islam, M. T. Islam, P. Kirawanich, and M. S. Soliman, "FT-FEDTL: A fine-tuned feature-extracted deep transfer learning model for multi-class microwave-based brain tumor classification," *Computers in Biology and Medicine*, Vol. 183, 109316, 2024.

[18] Gupta, H., V. Maheshwari, and V. V. Thakery, "Brain tumor detection by microwave imaging using planner antenna," *International Journal of Bio-Science and Bio-Technology*, Vol. 8, No. 5, 201–210, 2016.

[19] Chandra, R. and I. Balasingham, "Detection of brain tumor and localization of a deep brain RF-source using microwave imaging," in *2015 9th European Conference on Antennas and Propagation (EuCAP)*, 1–5, 2015.

[20] Asok, A. O., R. Anjaly, N. Kunju, and S. Dey, "Microwave medical imaging using a compact monopole antenna for brain tumor detection," in *2023 First International Conference on Microwave, Antenna and Communication (MAC)*, 1–4, IEEE, 2023.

[21] Särestöniemi, M., D. Singh, R. Dessai, C. Heredia, S. Myllymäki, and T. Myllylä, "Realistic 3D phantoms for validation of microwave sensing in health monitoring applications," *Sensors*, Vol. 24, No. 6, 1975, 2024.

[22] Groumpas, E., M. Koutsoupidou, I. S. Karanasiou, C. Papageorgiou, and N. Uzunoglu, "Real-time passive brain monitoring system using near-field microwave radiometry," *IEEE Transactions on Biomedical Engineering*, Vol. 67, No. 1, 158–165, 2019.

[23] Hossain, A., M. T. Islam, S. K. A. Rahim, M. A. Rahman, T. Rahman, H. Arshad, A. Khandakar, M. A. Ayari, and M. E. H. Chowdhury, "A lightweight deep learning based microwave brain image network model for brain tumor classification using reconstructed microwave brain (RMB) images," *Biosensors*, Vol. 13, No. 2, 238, 2023.

[24] Inum, R., M. M. Rana, K. N. Shushama, and M. A. Quader, "EBG based microstrip patch antenna for brain tumor detection via scattering parameters in microwave imaging system," *International Journal of Biomedical Imaging*, Vol. 2018, No. 1, 8241438, 2018.

[25] Gupta, H. K., R. Sharma, and V. V. Thakre, "Tumor detection in multilayer brain phantom model by symmetrical-shaped DGS rectangular microstrip patch antenna," in *International Conference on Intelligent Computing and Smart Communication 2019: Proceedings of ICSC 2019*, 705–712, 2020.

[26] Shokry, M. A. and A. M. M. A. Allam, "UWB antenna for brain stroke and brain tumour detection," in *2016 21st International Conference on Microwave, Radar and Wireless Communications (MIKON)*, 1–3, IEEE, 2016.

[27] Raihan, R., M. S. A. Bhuiyan, R. R. Hasan, T. Chowdhury, and R. Farhin, "A wearable microstrip patch antenna for detecting brain cancer," in *2017 IEEE 2nd International Conference on Signal and Image Processing (ICSIP)*, 432–436, IEEE, 2017.

[28] Saleeb, D. A., R. M. Helmy, N. F. F. Areed, M. Marey, W. M. Abdulkawi, and A. S. Elkorany, "A technique for the early detection of brain cancer using circularly polarized reconfigurable antenna array," *IEEE Access*, Vol. 9, 133 786–133 794, 2021.

[29] Nair, V. V., E. George, and A. James, "Real-time tumor detection using electromagnetic signals with memristive echo state networks," *IEEE Internet of Things Journal*, Vol. 11, No. 20, 33 712–33 721, 2024.

[30] Sharma, M. K., M. Kumar, J. P. Saini, D. Gangwar, B. K. Kanaujia, S. P. Singh, and A. Ekuakille, "Experimental investigation of the breast phantom for tumor detection using ultra-wide band-MIMO antenna sensor (UMAS) probe," *IEEE Sensors Journal*, Vol. 20, No. 12, 6745–6752, 2020.

[31] Saleeb, D. A., R. M. Helmy, N. F. F. Areed, M. Marey, K. M. Almustafa, and A. S. Elkorany, "Detection of kidney cancer using circularly polarized patch antenna array," *IEEE Access*, Vol. 10, 78 102–78 113, 2022.

[32] Al-Gburi, A. J. A., I. Ibrahim, and Z. Zakaria, "A miniature raspberry shaped UWB monopole antenna based on microwave imaging scanning technique for kidney stone early detection," *Int. J. Psychosoc. Rehabil*, Vol. 24, No. 2, 1755–1763, 2020.